electronics

MDPI

Article

Reduction of Human Interaction with Wireless Power Transfer System Using Shielded Loop Coil

Akihiko Kumazawa [1], Yinliang Diao [2], Akimasa Hirata [2] and Hiroshi Hirayama [2,*]

1 Tokai Rika, 3-260 Toyota, Oguchi-cho, Niwa-gun, Aichi 480-0195, Japan; hirayama_hiroshi@m.ieice.org
2 Graduate School of Engineering, Nagoya Institute of Technology, Gokiso-cho, Showa-ku, Nagoya, Aichi 466-8555, Japan; diao.yinliang@nitech.ac.jp (Y.D.); ahirata@nitech.ac.jp (A.H.)
* Correspondence: hirayama@nitech.ac.jp; Tel.: +81-52-735-5448

Received: 13 May 2020; Accepted: 1 June 2020; Published: 8 June 2020

Abstract: The impedance variation of wireless power transfer (WPT) coils owing to the presence of the human body may result in mismatches, resulting in a decrease of the transmission efficiency. In addition, one of the decisive factors of the permissible transfer power in WPT systems is a compliance assessment with the guidelines/standards for human protection from electromagnetic fields. In our previous study, we reported that a shielded loop coil can potentially reduce human interaction with WPT coils. In this study, first, the rationale for this reduction is investigated with equivalent circuit models for a WPT system using a shielded loop coil operated in close proximity to the human body. We then conducted an equivalent circuit analysis considering the capacitance between the inner and outer conductors of the shielded loop coil, suggesting the stability of the impedance matching. From computational results, the mitigation capability of the shielded loop coil on impedance matching and transmission efficiency owing to the presence of the human body was verified for 6.78 MHz wireless power transfer. Additionally, the reduction of the specific absorption rate (SAR) with coils comprised of the shielded loop structure was confirmed in the presence of anatomically realistic human body models. The maximum transferable power was increased from 1.5 kW to 2.1 kW for the restrictions of the local SAR limit prescribed in the international safety guidelines/standard.

Keywords: shielded loop coil; wireless power transfer; SAR; coupled resonance

1. Introduction

Wireless power transfer (WPT) technology is being put to practical use in various places [1–3]. For example, it will be deployed for the wireless charging of electric vehicles in parking areas [4–7]. When new emerging technology may appear, there has been concern about electromagnetic compatibility issues, which are mainly classified into two categories: potential health effects of electromagnetic fields and unwanted field emissions. Unlike other devices used in wireless communications, the leaked field strength from WPT systems is non-negligible even for high transmission efficiency because of potentially high power transfer [8,9]. The above mentioned two issues should thus be considered carefully.

Unwanted field emissions are related to the assessment of the far-field strength, whereas the compliance assessment of human safety standards is more related to near-field issues. Our interest here focuses on the latter. Human safety assessment is also related to the performance of power transfer in close proximity to the human body. Specifically, the presence of the human body may result in a mismatch in the input impedance of the transmitting/receiving coils, resulting in degraded transmission efficiency [10,11]. The method of reducing this interaction may be related to human safety because compliance assessments are, in general, conducted in a worst-case exposure, and thus in a certain scenario where the impedance mismatch occurs.

In the International Commission on Non-Ionizing Radiation Protection (ICNIRP) guidelines and IEEE standard [12–14] for human protection from electromagnetic fields, two metrics are mentioned: basic restrictions and reference levels. The former involves the internal physical quantities which are related to adverse health effects with a certain reduction factor. The latter is the permissible external field strength, which is derived from basic restrictions in a conservative manner. Practically, the reference level for a near-field regime is conservative by one to two orders of magnitude. At frequencies higher than 100 kHz, the physical quantity representing the basic restriction is the specific absorption rate (SAR) averaged over 10 g of tissue. Note that the internal electric field strength should also be evaluated up to 10 MHz, although the former would be dominant for continuous (non-pulse) exposure in the MHz frequency range. Thus, the evaluation of the local spatial-averaged SAR and internal electric field is crucial in a WPT system design.

Many studies have investigated electromagnetic safety issues owing to the exposure to magnetic fields generated by WPT systems [15–22]. Chen et al. [15] evaluated the induced electric field in a human body model exposed to a prototype WPT system of 5 W which received power from 0.1 MHz to 10 MHz. Shimamoto et al. [19] investigated the discrepancies in the electric field in a human body with different postures. The differences in the SAR between adult and child models were studied for a WPT system at 6.78 MHz [20]. In [21,22], the coupling factor, which relates the peak in situ electric field with an applied nonuniform magnetic field, was calculated. Zhan et al. [23], Campi et al. [24], Park et al. [25] and Kim et al. [26] proposed methods such as compensation topology and a passive shield to reduce the leakage magnetic field of WPT systems, while Nadakuduti et al. [27] and Ishihara et al. [28] investigated the relevant measurement methodologies. The above mentioned studies mainly focused on the safety aspects of WPT systems but did not consider the effects of the presence of the human body on the WPT performance based on a worse-case scenario.

A shielded loop antenna has two significant functions. One is a self-balancing effect to decrease sensibility to an electric field of its feeding line [29]. To take advantage of this, the shielded loop antenna has been widely used for broadcasting reception to eliminate electric field noise [30,31]. The shielded loop antenna is also used as a sensor of magnetic fields [32–34] to ensure measurement accuracy [35]. The other is a mitigation effect from surrounding metallic objects [36]. The shielded loop antenna was first invented for direction finding systems to overcome degradation of directivity pattern due to the proximity of an external object (such as a metallic wall) [37]. To take advantage of this, the shielded loop antenna is also widely used for magnetic resonance imaging (MRI) to prevent the detune of resonant frequency due to a presence of human body [37–42]. Considering this evidence, it is expected that the use of a shielded loop coil in a WPT system has a capability of mitigating the detune effect due to presence of a human body.

Previously, we empirically presented a near-field WPT using a shielded loop coil [42]. This WPT had potential features of high transmission efficiency and reduction of external electric fields, which may be expected with the presence of the human body. However, the rationale for these features is unclear, especially for a realistic exposure scenario where the human body exists. In this study, we first develop an equivalent circuit model of a 6.78 MHz WPT system composed of shielded loop coils to demonstrate its capability. We then demonstrate that the impedance characteristics and the SAR reduction of a shielded loop coil are improved as compared to a conventional loop coil without a shield. The permissible field strength is evaluated based on computations using an anatomically based human model.

2. Simulation Model

To evaluate the WPT coil performance in the presence of a human body model, the commercial software FEKO (Altair, hyperworks, Michigan, MI, USA) was used. The structure of a shielded loop coil is shown in Figure 1a,b. The shielded loop coil is well-known and commonly used as a magnetic field sensor because of its ability to suppress the sensibility of electric fields [29]. A gap was made to suppress only the electric field without suppressing the magnetic field, as is common in a shielded loop coil [43]. Because of the gap, there was no current flow in the outer conductor, and thus current flows only in the inner conductor. The outer conductor acted as a shield for the electric field.

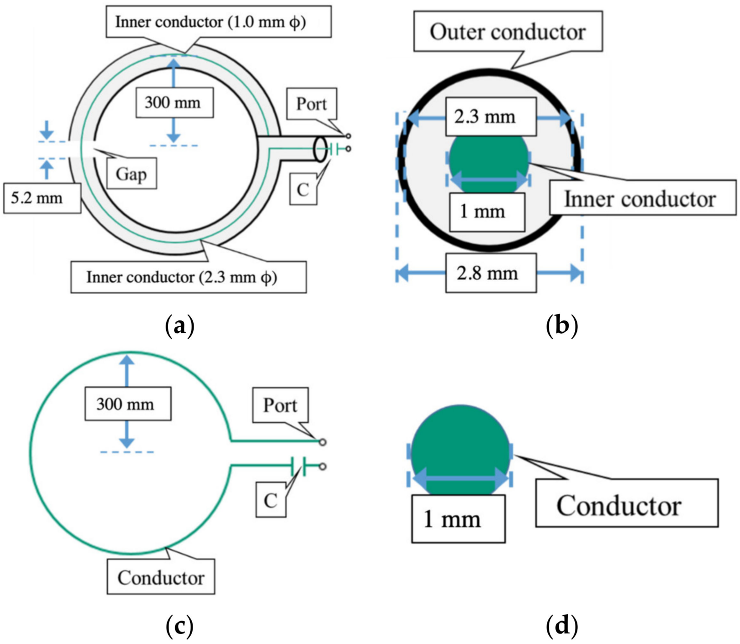

Figure 1. Schematic explanation of a shielded loop coil. (**a**) Overall view of a shielded loop coil, (**b**) sectional view of a shielded loop coil, (**c**) overall view of a one-turn loop coil, and (**d**) sectional view of a one-turn loop coil.

To verify the effectiveness of the WPT system composed of a shielded loop coil, a one-turn loop coil was also considered. The size of the one-turn loop coil is identical to that of the shielded loop coil, as shown in Figure 1c. The outer diameter of the conductor in the one-turn loop coil is identical to that of the shielded loop coil, as shown in Figure 1d.

The simple one-turn shielded loop structure was employed in this paper in order to evaluate basic characteristics of using a shielded loop structure for WPT. In a practical use, a multi-turn shielded loop [37] is effective to improve inductance and the coupling coefficient.

In this paper, the shielded loop structure is assumed to be made of shielded cable. In actual use, a shielded loop structure can be realized by using a printed circuit board (PCB) [44].

To discuss the electric field suppressing effect of the shielded loop coil, a one-turn loop coil with a parallel capacitance was also considered. This parallel capacitance simulates the capacitance between the inner and the outer conductors of the shielded loop coil.

For each model, capacitors were connected in series to each coil to resonate at 6.78 MHz. The same structure was used on the transmitting (Tx) and receiving (Rx) sides. By using a method-of-moment (MoM) simulation, the input impedances of these models were calculated. In a numerical simulation, the copper was assumed as a conductor, and then its conductivity of 5.81×10^6 S/m was assigned. An AC power supply with an output impedance of 50 Ω was connected to the port of the Tx side. A resistance of 50 Ω was loaded to the port of the Rx side. Delta-gap feeding was applied at the port in the MoM simulation.

An equivalent circuit was employed to understand the impedance matching mechanism of the shielded loop coil. Equivalent circuits of the coils are shown in Figure 2. For the one-turn loop coil shown in Figure 2a, the coil was modeled by an inductor whose inductance was derived by the MoM simulation at a low frequency (100 kHz). A series capacitance C_{S1} = 223.3 pF was determined so that the imaginary part of the input impedance becomes zero at 6.78 MHz. For the shielded loop coil shown in Figure 2b, the inductance of the equivalent circuit was calculated from the MoM simulation at a low frequency (100 kHz); this was identical to the value of the one-turn loop coil because the current flows only in the inner conductor of the shielded loop, which is the same structure as that of the one-turn loop coil. A series capacitance C_{s2} = 157.2 pF represents the stray capacitance between the inner and outer conductors, and was calculated by the self-resonant frequency through the MoM simulation.

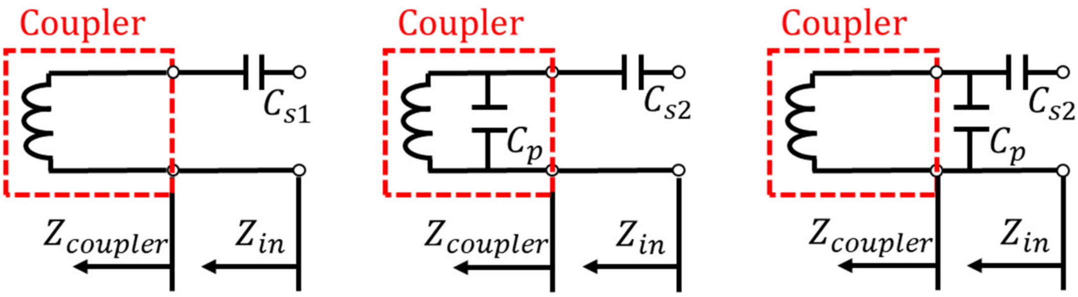

(**a**) (**b**) (**c**)

Figure 2. Equivalent circuits of different coils. (**a**) One-turn loop coil, (**b**) shielded loop coil, and (**c**) one-turn loop with capacitor.

For the one-turn loop coil with a shunt capacitor shown in Figure 2c, the equivalent circuit is identical to the shielded loop. It is noteworthy that the shunt capacitor of the one-turn loop was realized by a discrete capacitor, while the shunt capacitor of the shielded loop was realized by a stray capacitance. The aim of the equivalent circuit analysis is to understand the impedance matching mechanism of the shielded loop coil. Thus, only the imaginary part of the impedance was considered.

C_{S1} and C_{S2} are optimized without the human body. These values are maintained when the human body is present. Since C_p represents the stray capacitance of the shield structure itself, this value is not varied by the human body. Input impedance Z_{in} for these models, calculated by MoM and the equivalent circuit, is shown in Figure 3. The estimation error of the equivalent circuit was calculated by using the root mean square percentage error (RMSPE) [45]:

$$\text{RMSPE} = \sqrt{\frac{1}{N}\sum\left(\frac{Im\left\{Z_{in}^{MoM}\right\} - Im\left\{Z_{in}^{Eq}\right\}}{Im\left\{Z_{in}^{MoM}\right\}}\right)^2} \times 100 \quad (1)$$

where Z_{in}^{MoM} and Z_{in}^{Eq} are the input impedances calculated by MoM and the equivalent circuit, respectively. N is the number of calculation frequencies. Consequently, the RMSPE of the one-turn loop, one-turn loop with C_p, and shielded loop was 1.61%, 3.97%, and 4.75%, respectively. Considering that the estimation error becomes large when the denominator of Equation (1) (i.e., $Im\left\{Z_{in}^{MoM}\right\}$) is zero, the input impedance calculated by the equivalent circuit is in good accordance with that calculated by MoM.

A schematic explanation of the power transfer scenario is shown in Figure 4. To calculate the input impedance and transmission efficiency, a homogeneous cylinder model composed of 2/3 muscle tissue was used as a canonical human body [46], as shown in Figure 4a.

To calculate the internal electric field and SAR, Japanese male model "TARO" developed by National Institute of Information and Communications Technology (Japan), shown in Figure 4b, was also considered [47]. The height and weight were 1.73 m and 65 kg, respectively; and the number of tissues is 51. The spatial resolution of the body model was 2 mm. The separation between the coils and human body was set to be 2 cm. This separation distance assuming the worst-case where the receiving coil was set on a laptop computer and the transmitting coil was set on a desk. The tissues conductivities were adopted from [48], and those of selected tissues at 6.78 MHz are listed in Table 1.

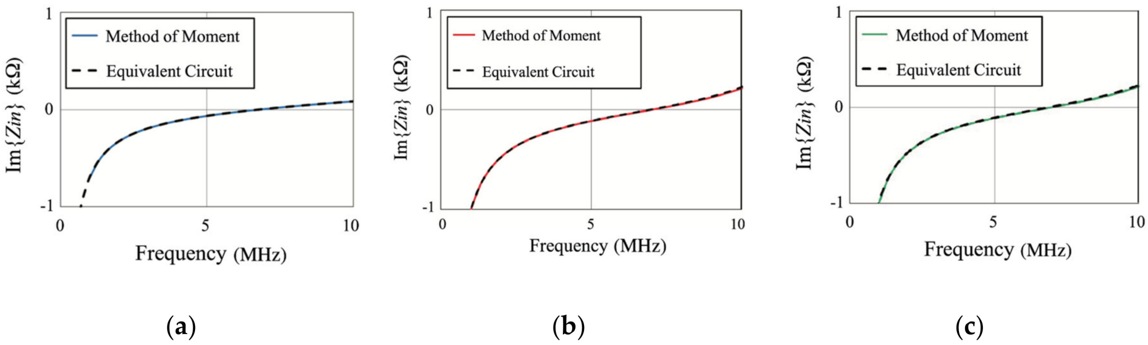

Figure 3. Input impedances calculated by Method-of-Moment (MoM) and equivalent circuit. (**a**) One-turn loop coil, (**b**) shielded loop coil, and (**c**) one-turn loop with capacitor.

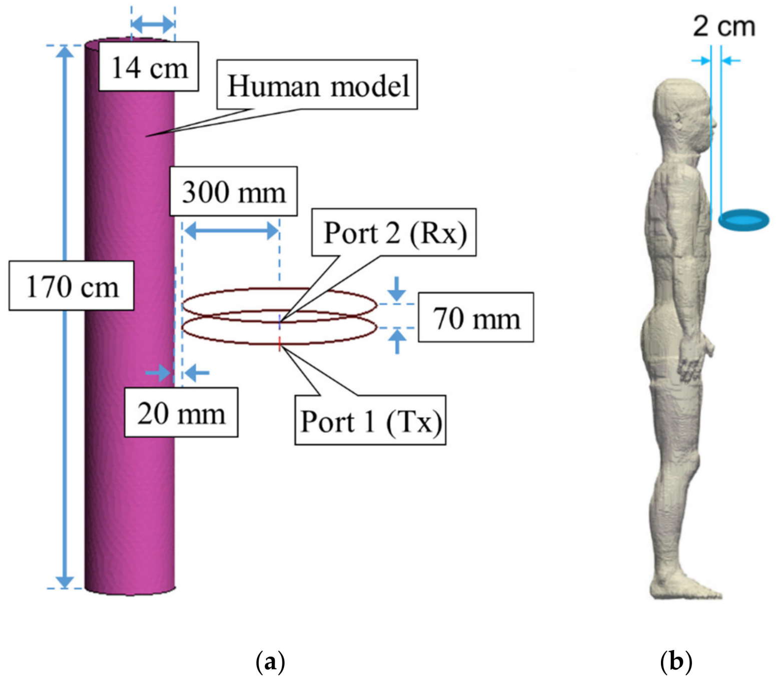

Figure 4. Simulation model of a shielded loop coil in the presence of a cylindrical model imitating a human body. (**a**) Simple cylindrical model and (**b**) realistic human body model.

Table 1. Electrical Conductivities of selected tissues of TARO model at 6.78 MHz.

Tissue	Conductivity (S/m)	Tissue	Conductivity (S/m)
Skin	0.1471	Heart	0.4713
Muscle	0.6021	Liver	0.2936
Fat	0.0278	Lung	0.3157
Bone(cortical)	0.0393	Kidney	0.4663
Bone(cancellous)	0.1159	Stomach	0.7575
Cartilage	0.3501	Cerebellum	0.3147
Nerve	0.2064	Tendon	0.4021
Grey matter	0.2520	Gall bladder	0.9013
White matter	0.1415	CSF	0.1415

At frequencies up to 10 MHz, Maxwell's equations can be simplified with a quasistatic approximation [48]. As a calculation method, an in-house multigrid-based scalar potential finite difference method was used [49,50] to solve the following partial differential equation:

$$\nabla\cdot[\sigma(-\nabla\varphi - j\omega \boldsymbol{A}_0)] = 0 \quad (2)$$

where boundary condition $\mathbf{n}\cdot(\nabla\varphi + \mathrm{j}\omega \boldsymbol{A}_0) = 0$. $\boldsymbol{A}_0$ and σ denote the magnetic vector potential of the applied magnetic field and the tissue conductivity, respectively. The vector potential $\boldsymbol{A}_0$ was obtained directly from the magnetic field, which was calculated by the method of moment. In this study, the scalar potential was computed iteratively via the successive-over-relaxation and multigrid methods [50]. The iteration stopped when the relative residual was less than 10^{-6}. When Equation (1) was solved, the in situ electric field (E) was calculated as $\boldsymbol{E} = -\nabla\varphi - \mathrm{j}\omega\boldsymbol{A}_0$. The in situ electric field and SAR averaged over 10 g of tissue, which are metrics for the compliance assessment prescribed in the exposure guidelines/standards, and were analyzed.

3. Simulation Result

3.1. Mitigation Effect of a Shielded Loop Coil on Impedance Matching Owing to the Existence of a Human Body

By using the scenario shown in Figure 4a, the input impedances of the coils were calculated. The calculated results are shown in Figure 5. From this figure, better impedance matching was achieved in the shield structure than that of the conventional one-turn loop coil. In addition, the impedance of the one-turn loop coil with C_p presents almost identical behavior to that of the shielded loop coil, suggesting that impedance matching of the shielded loop coil was achieved by the stray capacitance between the inner and outer conductors.

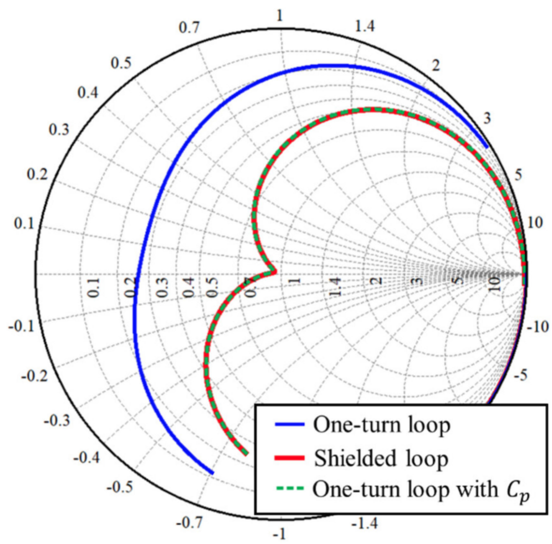

Figure 5. Smith chart of input impedance of loop coils.

To precisely discuss the effect of the human body, the reflection coefficients of the loop coil with C_p and the shielded loop coil with and without the simple cylindrical model are listed in Table 2. The variation of the reflection coefficient owing to the existence of the human body for the shielded loop coil was 0.14 dB, whereas that of a loop with C_p was 0.16 dB. From this result, the shielded loop coil can mitigate the impedance mismatch effect because the shielded loop coil can suppress the electric field.

Table 2. Reflection coefficients with and without simple cylindrical model.

Model	Shielded	Loop with C_p
Without human body model	−30.69 dB	−29.34 dB
Human body model	−30.83 dB	−29.50 dB
Variation owing to the human body	0.14 dB	0.16 dB

3.2. Transmission Efficiency

To evaluate the transmission efficiency, S parameters were calculated by using method-of-moment simulation. The scenario shown in Figure 4a was assumed, in which the transmitting and receiving coils had port 1 and 2, respectively. The frequency characteristics of the S parameters of these coils are shown in Figure 6 when the cylindrical model was present. Assuming a source and load impedance of 50 Ω, S_{21} represents the transmission efficiency. The transmission efficiency of the shielded loop coil was improved compared to the one-turn loop coil.

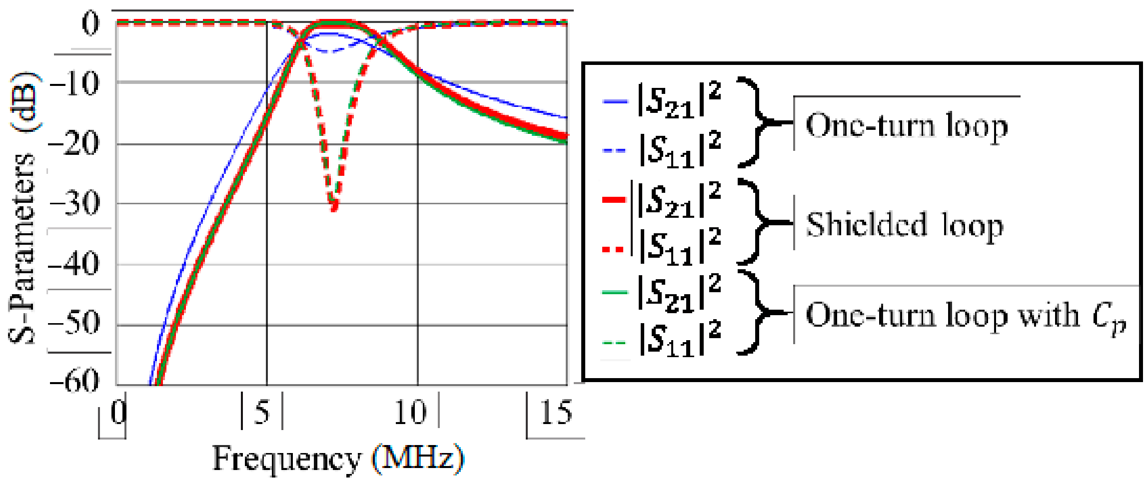

Figure 6. S parameters for frequencies of different coils.

The transmission efficiencies of the shielded loop coil and the one-turn loop with C_p were almost identical. Therefore, the transmission efficiency can be confirmed to be improved by the capacitance between the inner and outer conductors of the shield structure.

The transmission efficiencies of these coils calculated from the S parameters are listed in Table 3. The transmission efficiency of the shielded loop coil was improved by 49.5% compared to that of the one-turn loop coil. This is because of the impedance matching effect of the shielded loop coil. The transmission efficiency of the shielded loop coil was improved by 0.004 points compared to that of the one-turn loop coil with C_p. This is because of the mitigation effect on the impedance matching of the shielded loop coil.

Table 3. Transmission efficiency and transmitting power (P_T) for 1 W reception at a resonant frequency of 6.78 MHz.

Type of Coil	$\lvert S_{21}\rvert^2$	P_T (W)
One-turn loop coil	0.648	4.80
Shielded loop coil	0.969	2.12
One-turn loop with C_p	0.965	2.14

Transmitting power (P_T) was supplied from the power source to the Tx coil so that power of 1 W was received at a 50 Ω load at the terminal of the Rx coil. P_T is listed in Table 3. P_T of the shielded loop coil (2.12 W) was reduced by 55.8% compared to the one-turn loop coil (4.80 W). P_T of the shielded loop coil was reduced by 0.93% compared to the one-turn loop with C_p (2.14 W).

3.3. Reduction Effect of SAR

By using a realistic human body model, the induced electric field distribution and local SAR distribution were calculated at a 1 W reception power for all three types of coils at a resonant frequency of 6.78 MHz. The efficiencies and transmitting powers are listed in Table 3.

Figure 7 shows the induced electric field distributions. In all cases, hotspots appear around the outmost layers of the chest, which was the body part closest to the transmission coil. High electric fields could also be observed in the armpit region; this is attributable to the skin-to-skin contact [51]. When the electric fields passed through the interface of tissue layers with high-low-high conductivity contrast, a high electric field could be observed in the less conductive tissue layer. At 6.78 MHz, the conductivity of dry skin was about five times that of the hypodermis, resulting in a high in situ electric field strength in the hypodermis of the armpit region.

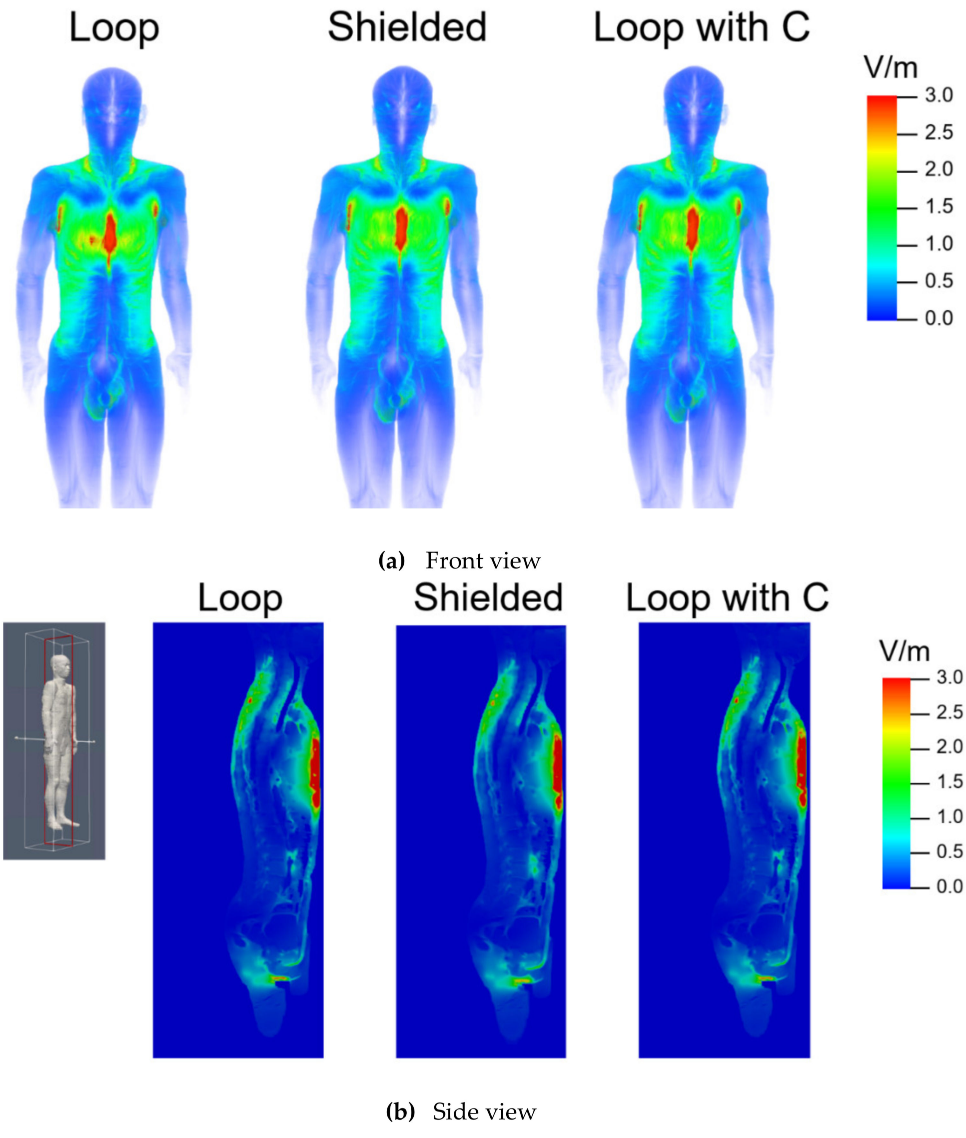

Figure 7. Internal electric field distribution in human body.

The maximum electric field strengths are 13.78 V/m, 11.88 V/m, and 11.85 V/m for the one-turn loop, shielded loop, and loop with capacitor, respectively. The maximum electric field strengths were reduced by 14.0% and 13.8% for the shielded loop coil and the loop coil with a capacitor compared to the loop coil. Figure 8 shows the SAR distributions in the human body model. The peak 10 g averaged SARs were 1.3 mW/kg, 0.94 mW/kg, and 0.93 mW/kg for the one-turn loop, shielded loop, and loop with capacitor, respectively. The SARs for the shielded loop coil and loop with capacitor were reduced by 27.9% and 27.8%, respectively, compared to that of the loop coil.

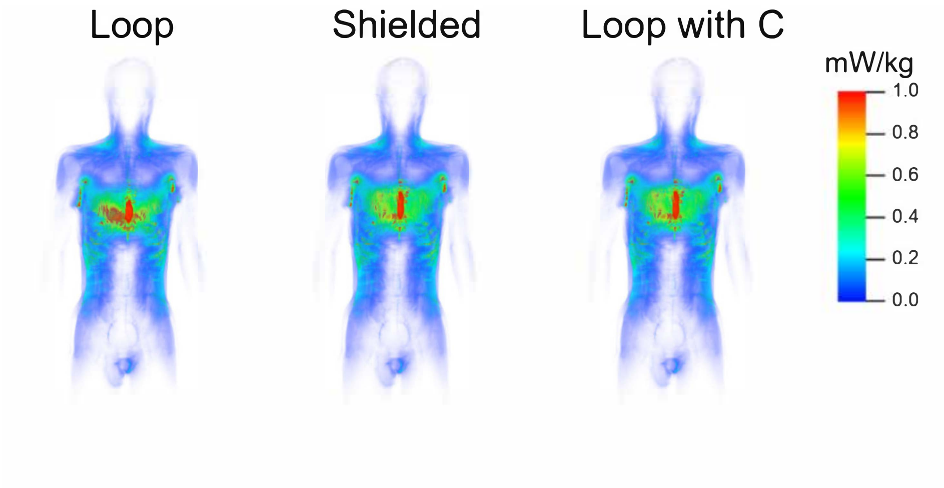

(**a**) Front view

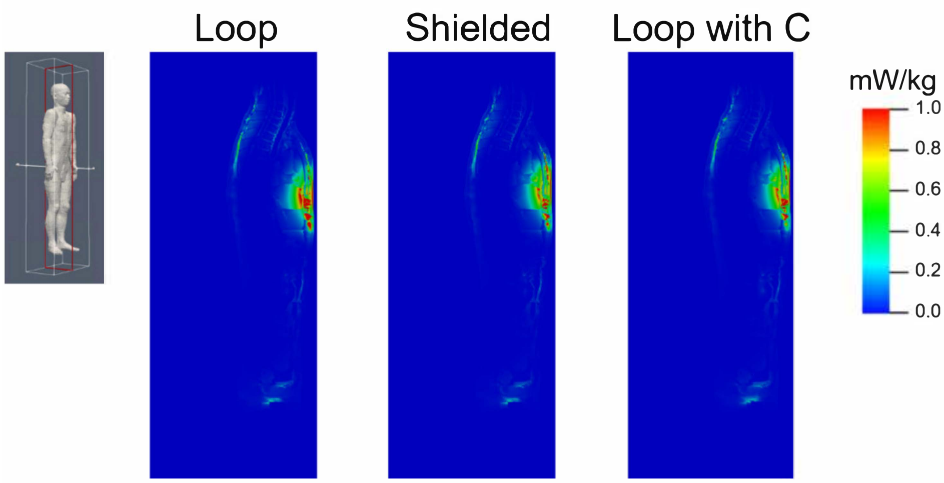

(**b**) Side view

Figure 8. Local SAR (Specific Absorption Rate) distribution in the human body.

4. Discussion

In this study, we proposed using a shielded loop structure as a coil in a WPT system. Our motivation was based on the fact that this structure is known to suppress the electric field distribution, resulting in interaction with the human body model. We then clarify this with an equivalent circuit model explaining why this structure may suppress the human–coil interaction. For comparison, we presented a one-turn loop coil model with a capacitance, demonstrating that the structure is comparable to that of the shielded loop coil. We also computationally demonstrated that the proposed structure can mitigate the interaction of the human body.

Although the equivalent circuits of the shielded loop coil and the one-turn loop coil with capacitance are identical, their electric field distributions are not identical. The shielded loop structure can mitigate input impedance fluctuations. Thus, the difference between the shielded loop structure and one-turn loop structure with the capacitance becomes much larger. In addition, a one-turn loop structure was considered in this study for practical application as well as for simplicity. If a helix structure is considered, the contribution of the electric field becomes large [52], resulting in greater interaction with the human body model. Again, the shielded loop structure is more stable than a conventional loop coil.

For human safety compliance, there are two metrics to be evaluated at 6.78 MHz: the internal electric field for preventing electrostimulation and the SAR for heating. For compliance analysis in terms of the in situ electric field, the metric is the 99th-percentile value of a 2 mm cubically averaged rms electric field strength in a specific tissue. Recent studies [53–56] revealed that for nonuniform exposure, the 99th-percentile value may underestimate the in situ field, and a value >99.9 was suggested based on statistical analysis. In this study, the 99.9th-percentile value of the electric field in skin is considered as the quantity to be compared with the basic restriction for a slightly more conservative estimation. The result for the shielded loop coil is found to be 2.97 V/m.

According to ICNIRP [56], the in situ electric field at 6.78 MHz should not exceed 915.3 V/m, and the 10 g averaged SAR should be below 2 W/kg for the general public. Based on the computed values for the shielded loop coil, we found that the maximum transferable powers are 94.98 kW and 2.1 kW. These calculations applied basic restrictions of the in situ electric field and SAR, respectively, suggesting that the heating effect is dominant for the scenario considered here. This is consistent with the findings of previous studies [15,20,57]. For the one-turn loop coil, the maximum transferable power is 1.5 kW when applying the SAR limit.

In our simulations, the separation between the torso and the border of the coil is set to be 2 cm, which is much smaller compared to the generally used measuring distance (mostly 20 or 30 cm) specified in IEC (International Electrotechnical Commission) 62,233 [58] for determining the electromagnetic field around household appliances. For a WPT, such standardization is currently undergoing, and it has not been well defined. Nonetheless, the calculated values can provide a rough (more conservative) estimate of the exposure doses for a WPT device with similar configurations.

5. Conclusions

In this study, the mitigation capability of a shielded loop coil on impedance matching and transmission efficiency owing to the presence of the human body for a 6.78 MHz wireless power transfer was verified based on the suppression of the electric field. Additionally, an induced electric field and SAR reduction effect of the shielded loop coil were confirmed.

Author Contributions: Funding acquisition, H.H.; Investigation, A.K. and Y.D.; Methodology, H.H.; Project administration, H.H.; Supervision, A.H. and H.H.; Visualization, A.K. and Y.D.; Writing—original draft, A.K. and Y.D.; Writing—review and editing, A.H. and H.H. All authors have read and agreed to the published version of the manuscript.

Funding: This research was supported by JSPS KAKENHI Grant Number 18K04137.

Conflicts of Interest: The authors declare no conflict of interest.

References

1. Shinohara, N. Power without wires. *IEEE Microw. Mag.* **2011**, *12*, 64. [CrossRef]
2. Kim, H.-J.; Hirayama, H.; Kim, S.; Han, K.J.; Zhang, R.; Choi, J.-W. Review of Near-Field Wireless Power and Communication for Biomedical Applications. *IEEE Access* **2017**, *5*, 21264–21285. [CrossRef]
3. Arai, T.; Hirayama, H. Folded Spiral Resonator with Double-Layered Structure for Near-Field Wireless Power Transfer. *Energies* **2020**, *13*, 1581. [CrossRef]
4. Laakso, I.; Hirata, A. Evaluation of the induced electric field and compliance procedure for a wireless power transfer system in an electrical vehicle. *Phys. Med. Boil.* **2013**, *58*, 7583–7593. [CrossRef] [PubMed]
5. Kim, S.; Park, H.H.; Kim, J.; Kim, J.; Ahn, S. Design and Analysis of a Resonant Reactive Shield for a Wireless Power Electric Vehicle. *IEEE Trans. Microw. Theory Tech.* **2014**, *62*, 1057–1066. [CrossRef]
6. Buja, G.; Bertoluzzo, M.; Mude, K.N. Design and Experimentation of WPT Charger for Electric City Car. *IEEE Trans. Ind. Electron.* **2015**, *62*, 7436–7447. [CrossRef]
7. Campi, T.; Cruciani, S.; De Santis, V.; Maradei, F.; Feliziani, M. EMC and EMF safety issues in wireless charging system for an electric vehicle (EV). In Proceedings of the 2017 International Conference of Electrical and Electronic Technologies for Automotive, Torino, Italy, 15–16 June 2017; pp. 1–4.

8. Kong, S.; Bae, B.; Jung, D.H.; Kim, J.J.; Kim, S.; Song, C.; Kim, J.J.; Kim, J. An Investigation of Electromagnetic Radiated Emission and Interference from Multi-Coil Wireless Power Transfer Systems Using Resonant Magnetic Field Coupling. *IEEE Trans. Microw. Theory Tech.* **2015**, *63*, 833–846. [CrossRef]
9. Suzuki, M.; Ogawa, K.; Moritsuka, F.; Shijo, T.; Ishihara, H.; Kanekiyo, Y.; Ogura, K.; Obayashi, S.; Ishida, M. Design method for low radiated emission of 85 kHz band 44 kW rapid charger for electric bus. In Proceedings of the 2017 IEEE Applied Power Electronics Conference and Exposition (APEC), Tampa, FL, USA, 26–30 March 2017; pp. 3695–3701.
10. Hirayama, H.; Ozawa, T.; Hiraiwa, Y.; Kikuma, N.; Sakakibara, K. A consideration of electro-magnetic-resonant coupling mode in wireless power transmission. *IEICE Electron. Express* **2009**, *6*, 1421–1425. [CrossRef]
11. Laakso, I.; Tsuchida, S.; Hirata, A.; Kamimura, Y. Evaluation of SAR in a human body model due to wireless power transmission in the 10 MHz band. *Phys. Med. Boil.* **2012**, *57*, 4991–5002. [CrossRef]
12. International Commission on Non-Ionizing Radiation Protection. (ICNIRP)1,2 Guidelines for Limiting Exposure to Electromagnetic Fields (100 kHz to 300 GHz). *Health Phys.* **2020**, *118*, 483–524. [CrossRef]
13. Bailey, W.H.; Harrington, T.; Hirata, A.; Kavet, R.R.; Keshvari, J.; Klauenberg, B.J.; Legros, A.; Maxson, D.P.; Osepchuk, J.M.; Reilly, J.P.; et al. Synopsis of IEEE Std C95.1™-2019 "IEEE Standard for Safety Levels with Respect to Human Exposure to Electric, Magnetic, and Electromagnetic Fields, 0 Hz to 300 GHz". *IEEE Access* **2019**, *7*, 171346–171356. [CrossRef]
14. IEEE Std. *C95.1-2019, IEEE Standard for Safety Levels with Respect to Human Exposure to Radio Frequency Electromagnetic Fields, 0 Hz to 300 GHz*; IEEE: New York, NY, USA, 2019; pp. 1–312.
15. Chen, X.L.; Umenei, A.E.; Baarman, D.W.; Chavannes, N.; De Santis, V.; Mosig, J.R.; Kuster, N. Human Exposure to Close-Range Resonant Wireless Power Transfer Systems as a Function of Design Parameters. *IEEE Trans. Electromagn. Compat.* **2014**, *56*, 1027–1034. [CrossRef]
16. Christ, A.; Douglas, M.; Nadakuduti, J.; Kuster, N. Assessing human exposure to electromagnetic fields from wireless power transmission systems. *Proc. IEEE* **2013**, *101*, 1482–1493. [CrossRef]
17. Hong, S.; Cho, I.; Choi, H.; Pack, J. Numerical anlaysis of human exposure to electromagnetic fields from wireless power transfer systems. In Proceedings of the 2014 IEEE Wireless Power Transfer Conference, Jeju, Korea, 8–9 May 2014; pp. 216–219.
18. Sunohara, T.; Hirata, A.; Laakso, I.; Onishi, T. Analysis ofin situelectric field and specific absorption rate in human models for wireless power transfer system with induction coupling. *Phys. Med. Boil.* **2014**, *59*, 3721–3735. [CrossRef] [PubMed]
19. Shimamoto, T.; Laakso, I.; Hirata, A. In-situelectric field in human body model in different postures for wireless power transfer system in an electrical vehicle. *Phys. Med. Boil.* **2014**, *60*, 163–173. [CrossRef] [PubMed]
20. Shimamoto, T.; Iwahashi, M.; Sugiyama, Y.; Laakso, I.; Hirata, A.; Onishi, T. SAR evaluation in models of an adult and a child for magnetic field from wireless power transfer systems at 6.78 MHz. *Biomed. Phys. Eng. Express* **2016**, *2*, 027001. [CrossRef]
21. Sunohara, T.; Hirata, A.; Laakso, I.; De Santis, V.; Onishi, T. Evaluation of nonuniform field exposures with coupling factors. *Phys. Med. Boil.* **2015**, *60*, 8129–8140. [CrossRef]
22. Wake, K.; Laakso, I.; Hirata, A.; Chakarothai, J.; Onishi, T.; Watanabe, S.; De Santis, V.; Feliziani, M.; Taki, M. Derivation of Coupling Factors for Different Wireless Power Transfer Systems: Inter- and Intralaboratory Comparison. *IEEE Trans. Electromagn. Compat.* **2017**, *59*, 677–685. [CrossRef]
23. Zhang, W.; White, J.C.; Malhan, R.K.; Mi, C.C.; Mi, C.C. Loosely Coupled Transformer Coil Design to Minimize EMF Radiation in Concerned Areas. *IEEE Trans. Veh. Technol.* **2016**, *65*, 4779–4789. [CrossRef]
24. Campi, T.; Cruciani, S.; Maradei, F.; Feliziani, M. Near-Field Reduction in a Wireless Power Transfer System Using LCC Compensation. *IEEE Trans. Electromagn. Compat.* **2017**, *59*, 686–694. [CrossRef]
25. Park, J.; Kim, N.; Hwang, K.; Park, H.H.; Kwak, S.I.; Kwon, J.H.; Ahn, S. A Resonant Reactive Shielding for Planar Wireless Power Transfer System in Smartphone Application. *IEEE Trans. Electromagn. Compat.* **2017**, *59*, 695–703. [CrossRef]
26. Kim, M.; Kim, H.; Kim, N.; Jeong, Y.; Park, H.H.; Ahn, S. A Three-Phase Wireless-Power-Transfer System for Online Electric Vehicles with Reduction of Leakage Magnetic Fields. *IEEE Trans. Microw. Theory Tech.* **2015**, *63*, 3806–3813. [CrossRef]

27. Nadakuduti, J.; Douglas, M.; Lu, L.; Christ, A.; Guckian, P.; Kuster, N. Compliance Testing Methodology for Wireless Power Transfer Systems. *IEEE Trans. Power Electron.* **2015**, *30*, 1. [CrossRef]
28. Ishihara, S.; Onishi, T.; Hirata, A. Magnetic Field Measurement for Human Exposure Assessment near Wireless Power Transfer Systems in Kilohertz and Megahertz Bands. *IEICE Trans. Commun.* **2015**, *98*, 2470–2476. [CrossRef]
29. Libby, L.L. Special Aspects of Balanced Shielded Loops. *Proc. IRE* **1946**, *34*, 641–646. [CrossRef]
30. Swinyard, W.O. Measurement of Loop-Antenna Receivers. *Proc. IRE* **1941**, *29*, 382–387. [CrossRef]
31. IEEE. *186-1948-IEEE Standard Methods of Testing Amplitude-Modulation Broadcast Receivers*; IEEE: New York, NY, USA, 1949.
32. Hirayama, H.; Hayashi, H.; Kikuma, N.; Sakakibara, K. Estimation of poynting vector and wavenumber vector from near-magnetic-field measurement. In Proceedings of the 2006 12th International Symposium on Antenna Technology and Applied Electromagnetics and Canadian Radio Sciences Conference, Montreal, Canada, 16 July 2006; pp. 1–4.
33. Hirayama, H.; Kondo, H.; Kikuma, N.; Sakakibara, K. Visualization of emission from bend of a transmission line with Poynting vector and wave-number vector. *Proc. EMC Eur.* **2008**, *2008*, 1–4.
34. Hirayama, H.; Kikuma, N.; Sakakibara, K. An Estimation Method of Poynting Vector with Near-Magnetic-Field Measurement. *IEICE Trans. Electron.* **2010**, *E93c*, 66–73. [CrossRef]
35. Whiteside, H.; King, R. The loop antenna as a probe. *IRE Trans. Antennas Propag.* **1964**, *12*, 291–297. [CrossRef]
36. Harpen, M.D. The theory of shielded loop resonators. *Magn. Reson. Med.* **1994**, *32*, 785–788. [CrossRef]
37. Barfield, R. Some experiments on the screening of radio receiving apparatus. *J. Inst. Electr. Eng.* **1924**, *62*, 249–262. [CrossRef]
38. Gadian, D.; Robinson, F. Radiofrequency losses in NMR experiments on electrically conducting samples. *J. Magn. Reson.* **1979**, *34*, 449–455. [CrossRef]
39. Zabel, H.J.; Bader, R.; Gehrig, J.; Lorenz, W.J. High-quality MR imaging with flexible transmission line resonators. *Radiology* **1987**, *165*, 857–859. [CrossRef] [PubMed]
40. Vestergaard-Poulsen, P.; Thomsen, C.; Sinkjær, T.; Henriksen, O. Simultaneous31P NMR spectroscopy and EMG in exercising and recovering human skeletal muscle: Technical aspects. *Magn. Reson. Med.* **1994**, *31*, 93–102. [CrossRef]
41. Ruytenberg, T.; Webb, A.; Zivkovic, I. Shielded-coaxial-cable coils as receive and transceive array elements for 7T human MRI. *Magn. Reson. Med.* **2019**, *83*, 1135–1146. [CrossRef] [PubMed]
42. Kajiura, N.; Hirayama, H. Improvement of transmission efficiency using shielded-loop antenna for wireless power transfer. In Proceedings of the 2016 International Symposium on Antennas and Propagation (ISAP), Okinawa, Japan, 24–28 October 2016; pp. 52–53.
43. Thomas, E.M.; Heebl, J.D.; Pfeiffer, C.; Grbic, A. A Power Link Study of Wireless Non-Radiative Power Transfer Systems Using Resonant Shielded Loops. *IEEE Trans. Circuits Syst. Regul. Pap.* **2012**, *59*, 2125–2136. [CrossRef]
44. Tierney, B.B.; Grbic, A. Planar Shielded-Loop Resonators. *IEEE Trans. Antennas Propag.* **2014**, *62*, 3310–3320. [CrossRef]
45. Cagatay, B.; Serdar, D. Adaptive Weighted Performance Criterion for Artificial Neural Networks. In Proceedings of the International Conference on Artificial Intelligence and Data Processing (IDAP), Malatya, Turkey, 28–30 September 2018; pp. 1–4.
46. Gabriel, S.; Lau, R.W.; Gabriel, C. The dielectric properties of biological tissues: III. Parametric models for the dielectric spectrum of tissues. *Phys. Med. Boil.* **1996**, *41*, 2271–2293. [CrossRef]
47. Nagaoka, T.; Watanabe, S.; Sakurai, K.; Kunieda, E.; Watanabe, S.; Taki, M.; Yamanaka, Y. Development of realistic high-resolution whole-body voxel models of Japanese adult males and females of average height and weight, and application of models to radio-frequency electromagnetic-field dosimetry. *Phys. Med. Boil.* **2003**, *49*, 1–15. [CrossRef]
48. Hirata, A.; Ito, F.; Laakso, I. Confirmation of quasi-static approximation in SAR evaluation for a wireless power transfer system. *Phys. Med. Boil.* **2013**, *58*, N241–N249. [CrossRef]
49. Dawson, T.W.; Stuchly, M.A. Analytic validation of a three-dimensional scalar-potential finite-difference code for low-frequency magnetic induction. *Appl. Comput. Electromagnet. J.* **1996**, *11*, 72–81.
50. Laakso, I.; Hirata, A. Fast multigrid-based computation of the induced electric field for transcranial magnetic stimulation. *Phys. Med. Boil.* **2012**, *57*, 7753–7765. [CrossRef] [PubMed]

51. Reilly, J.P.; Hirata, A. Low-frequency electrical dosimetry: Research agenda of the IEEE International Committee on Electromagnetic Safety. *Phys. Med. Boil.* **2016**, *61*, R138–R149. [CrossRef] [PubMed]
52. Kraus, J.D.; Marhefka, R.J. *Antenna for All Applications*, 3rd ed.; McGraw Hill: New Jersey, NJ, USA, 2001.
53. Laakso, I.; Hirata, A. Reducing the staircasing error in computational dosimetry of low-frequency electromagnetic fields. *Phys. Med. Biol.* **2012**, *57*, N25–N34. [CrossRef] [PubMed]
54. Gomez-Tames, J.; Laakso, I.; Haba, Y.; Hirata, A.; Poljak, D.; Yamazaki, K. Computational Artifacts of the In Situ Electric Field in Anatomical Models Exposed to Low-Frequency Magnetic Field. *IEEE Trans. Electromagn. Compat.* **2017**, *60*, 589–597. [CrossRef]
55. Diao, Y.; Gomez-Tames, J.; Rashed, E.A.; Kavet, R.; Hirata, A. Spatial Averaging Schemes of In Situ Electric Field for Low-Frequency Magnetic Field Exposures. *IEEE Access* **2019**, *7*, 184320–184331. [CrossRef]
56. International Commission on Non-Ionizing Radiation Protection. Guidelines for limiting exposure to time-varying electric and magnetic fields for low frequencies (1 Hz–100 kHz). *Health Phys.* **2010**, *99*, 818–836.
57. Christ, A.; Douglas, M.G.; Roman, J.M.; Cooper, E.B.; Sample, A.; Waters, B.H.; Smith, J.R.; Kuster, N. Evaluation of Wireless Resonant Power Transfer Systems with Human Electromagnetic Exposure Limits. *IEEE Trans. Electromagn. Compat.* **2012**, *55*, 1–10. [CrossRef]
58. IEC. *Measurement Methods for Electromagnetic Fields of Household Appliances and Similar Apparatus with Regard to Human Exposure*; IEC 62233; International Electrotechnical Commission: Geneva, Switzerland, 2005.